Int J Mater Form (2013) 6:209–221
DOI 10.1007/s12289-011-1072-5

ORIGINAL RESEARCH

Characterization of the tool/fabric and fabric/fabric friction for woven-fabric composites during the thermostamping process

Konstantine A. Fetfatsidis · David Jauffrès · James A. Sherwood · Julie Chen

Received: 19 January 2011 / Accepted: 15 August 2011 / Published online: 22 November 2011

Abstract The dynamic coefficients of friction for Twintex® commingled glass-polypropylene balanced plain-weave and unbalanced twill-weave fabrics at the tool/fabric and fabric/fabric interfaces during the composite thermostamping process are characterized. The effects of fabric velocity and pressure on the coefficients of friction under conditions similar to those during the thermostamping process are studied. A phenomenological friction model accounting for pressure and velocity dependence is developed based on the experimental results and implemented into the commercial finite element codes ABAQUS/Explicit and LS-DYNA via user-defined subroutines. The mechanical behavior of the fabric is modeled using a mesoscopic approach. The friction subroutines are validated with a finite element model of the experimental friction test. The forming of a hemispherical dome is simulated using ABAQUS and LS-DYNA. Punch forces and yarn stresses are compared between variable friction and constant friction models, and the simulation results justify the necessity for a variable friction model to accurately predict part quality.

Keywords Thermostamping · Thermoforming · Woven-fabric · Composite forming

Introduction

The move from metal parts to composite parts by the automotive and aerospace industries is motivated by the need for increased fuel efficiency through reduced weight and these composite parts bring the additional benefits of fire- and corrosion-resistance. Thermostamping, sometimes called thermoforming, has been shown to be an attractive process for producing woven-fabric reinforced composite parts at a relatively low cost for high-volume production scenarios [1]. During the thermostamping process for the fabric system considered in the current research (Fig. 1 [2]), a fabric blank consisting of commingled reinforcing (fiberglass) and thermoplastic fibers (polypropylene) is preheated in an oven until the thermoplastic fibers melt and infuse the fiberglass. The fabric is then shuttled to a press where metal binder rings apply in-plane forces to prevent fabric wrinkling. A metal punch then presses the blank into a metal die cavity, where it is left for a few seconds to cool and solidify. As the fabric blank is pressed to conform to the shape of the die, the fabric slides against the metal tools, which include the binder rings, punch, and die. Additionally, multiple layers of woven-fabric composite blanks are usually stacked together with various orientations thereby resulting in relative motion between adjacent layers of fabric during the forming process.

Too much in-plane tension resulting from the binder can lead to yarn separation and fabric tearing, while too little in-plane tension may result in unwanted wrinkles in the fabric part [3]. As a result, a reliable simulation tool is valuable to determine the manufacturing process parameters, in particular the binder force, to make a quality part in minimal time. Such a simulation tool can eliminate or at least reduce the need for the trial-and-error approach that is often used in composite manufacturing. Several simulation tools accounting for the specific fabric mechanical behavior have been developed [4–10].

K. A. Fetfatsidis · D. Jauffrès · J. A. Sherwood (✉) · J. Chen
Department of Mechanical Engineering,
University of Massachusetts Lowell,
One University Ave.,
Lowell, MA 01854, USA
e-mail: james_sherwood@uml.edu

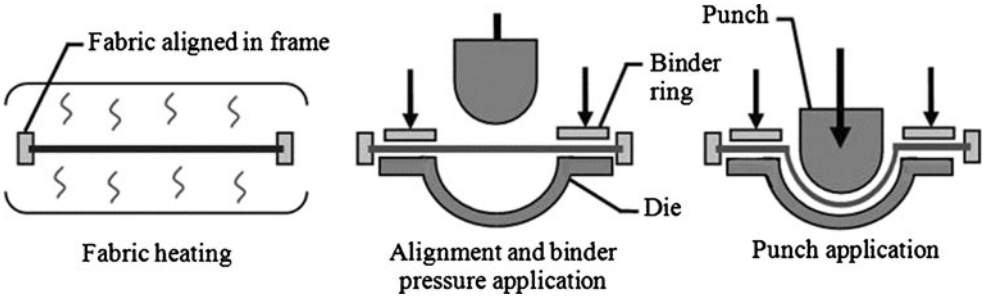

Fig. 1 Schematic of thermostamping/thermoforming process [2]

For the fabric system in the current research, the relative motion between the metal tooling and the fabric (tool/fabric) and between adjacent layers of fabric (fabric/fabric) induces friction, and the corresponding coefficient of friction can vary between 0.1 and 0.5 depending on punch velocity and the punch and binder forces [1, 3, 11]. In the absence of friction data, researchers performing thermoforming simulations have typically assumed a constant friction coefficient of 0.3 at the fabric/tool and fabric/fabric interfaces [4–6]. A robust simulation will account for the variation in the friction coefficients over the fabric throughout the duration of the forming process. The friction coefficient has been shown to greatly influence the punch force and resulting yarn tension. For example, for a hemisphere stamping simulation, the punch force is more than halved when using a friction coefficient of 0.1 versus the conventional 0.3 (Fig. 2 [12]).

Several attempts have been made to characterize the friction of woven-fabric composites [1, 11, 13–17]. The studied parameters are generally the fabric velocity and the pressure. The effects of fabric orientation, fabric shearing, and resin viscosity (through variations in tool and fabric temperatures) on the coefficient of friction have also been investigated. These parameters have also shown to have an effect on the coefficient of friction for many fabrics [13–15], but for the fabrics tested in the current research, only fabric velocity and pressure were observed to significantly influence the coefficient of friction under conditions similar to those found in the thermoforming process [12]. A phenomenological approach, using Stribeck theory, can combine the influences of pressure and velocity on the friction coefficient into one parameter. The Stribeck curve (Fig. 3) relates the Hersey number, $\boldsymbol{H}$, to the coefficient of friction, μ [18]. The Hersey number is a function of pressure, $\boldsymbol{P}$, velocity, $\boldsymbol{U}$, and temperature (through viscosity, η) and is given by,

$$H = \frac{\eta U}{P} \tag{1}$$

The Stribeck curve is divided into three regions indicating the degree of separation between contacting surfaces by a thin lubricant. It has been found that the coefficient of friction at the tool/fabric interface for the fabrics considered in this paper corresponds to the hydrodynamic region of the Stribeck curve [19]. Note that these findings assume the thickness of the thin lubricant remains constant for all combinations of velocity, pressure, and temperature and this assumption is likely an oversimplification and will be shown in this paper to be unnecessary. Also, many of the previous studies have

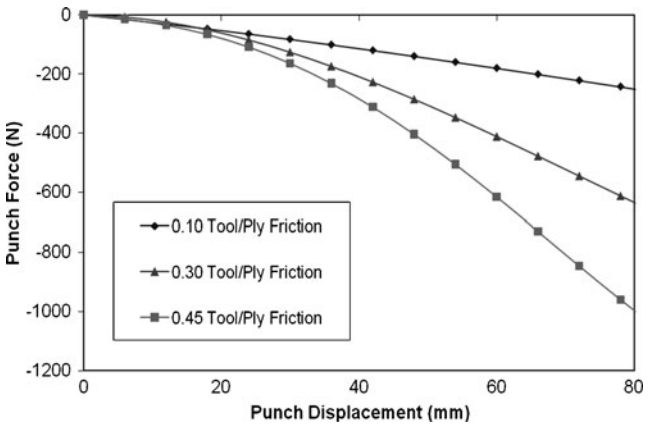

Fig. 2 Effect of varying tool/fabric friction on punch force (for fabric/fabric μ=0.3) for balanced plain-weave fabric [12]

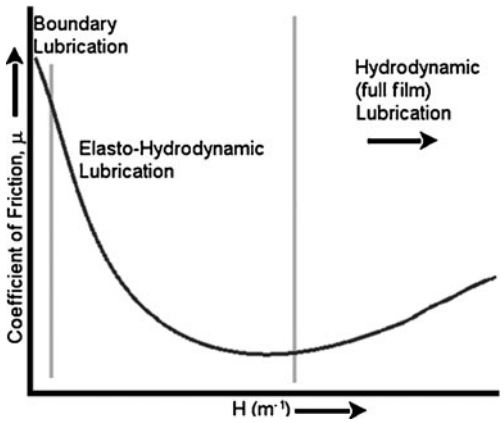

Fig. 3 Theoretical Stribeck curve

focused on the friction between only the tool and the fabric, and the conditions used during the tests have not completely represented the conditions used during the thermoforming process. In addition, very few attempts have been made to incorporate pressure and velocity dependence of the friction coefficient within a finite element code to simulate the thermoforming process [19, 20].

In the current study, the dynamic and static coefficients of friction at the tool/fabric and fabric/fabric interfaces are quantified using a constant-load friction-test apparatus [21]. Based on a varying fabric velocity and pressure, a phenomenological model using Stribeck theory is incorporated into the commercially available finite element codes ABAQUS/Explicit and LS-DYNA as a user-defined friction subroutine. The forming of a hemispherical dome is simulated using the ABAQUS and LS-DYNA explicit finite elements programs. Punch forces, and yarn stresses are compared between variable-friction and constant-friction models.

Experimental description

Material

Two Twintex® fabrics (commingled fiberglass/polypropylene fibers), commonly used in thermostamping, were investigated to quantify their frictional properties. The two fabrics differ in their weaving and yarn thickness, where the first one is a balanced plain weave with thin yarns and will be referred to as PW; and the second is an unbalanced twill-weave with thick yarns and will be referred to as TW. These fabrics were donated by Vetrotex (now owned by Owens Corning) and are part of an international benchmark exercise [22].

Experimental set-up

The apparatus used to measure the friction between the fabrics and the tool consists of two heated steel platens to replicate the steel tools used in thermoforming. The details on the friction test apparatus and validation of the setup are given in [21]. Using a closed-loop feedback control system that features three compression load cells and a pressure regulator, a constant normal force, N, is maintained on the top platen while a fabric sample (gripped inside a holder) is pulled from the pressed platens with a pull-out force, F (Fig. 4(a)). The effective coefficient of friction is calculated by

$$\mu_{eff} = \frac{F}{2N} \tag{2}$$

where the normal force is multiplied by a factor of two to account for the two contacting surfaces on each side of the fabric sample. The sample of fabric pulled out is smaller than the platen such that the surface area in contact and hence the pressure applied does not vary during the experiment. The pull-out force is plotted as a function of pull-out distance (Fig. 5), and an initial peak force needed to be overcome to initiate slipping is observed. This initial peak force corresponds to the static coefficient of friction. Following the initial peak is a somewhat steady-state value of the pull-out force corresponding to the dynamic coefficient of friction. The apparatus is configured such that fabric can be preheated to approximately 170°C using an infrared oven before being transferred in-between the platens, or the platens can be used to heat the samples to 170°C. The former (use of the oven) attempts to replicate the actual thermostamping process while the latter provides a potentially more uniform temperature for testing purposes. A thermocouple embedded into each sample is used to monitor the temperature throughout the test. During the thermoforming process, the fabric temperature is assumed to be between 160-170°C within the one second required to stamp the part [12], i.e. above the melting temperature of polypropylene (~150°C [23]).

To measure the fabric/fabric friction, one modification from the configuration used for the tool/fabric setup is made to the test apparatus. Two pieces of fabric are clamped together on one end, and these two pieces of fabric sandwich the fabric sample mounted in the fabric holder (Fig. 4(b)). As the platens close shut and the fabric inside the holder begins to pull, the "sandwich" clamp is blocked by the closed platens, thus allowing only the middle layer to be pulled through the test device. In addition to validation results provided in [21], measurements made by the friction test apparatus will be compared to measurements from other participants in an

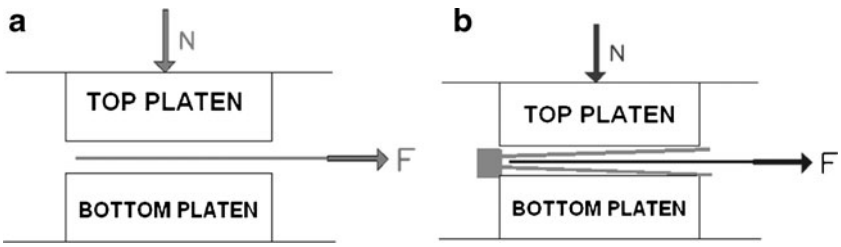

Fig. 4 **a** Schematic representation of the tool/fabric friction test setup and **b** the fabric/fabric friction test setup

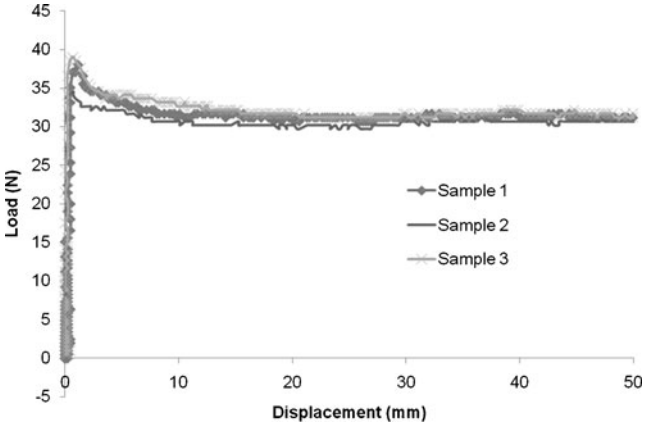

Fig. 5 Typical pull-out force vs. displacement curves resulting from friction experiments

ongoing international friction benchmark exercise. Preliminary results showed that for a set of test conditions (U= 60 mm/min, P=100 kPa, T=180°C), the measured static (0.17) and dynamic (0.14) coefficients of friction compared well to those measured by Sachs et al. [24] at the University of Twente (Fig. 6).

Modified Hersey number

Consider the physical definition of the Coulomb friction coefficient, μ, as the ratio of the frictional (shear) stress across an interface, $\tau = F/A$, where A is fabric surface area and F is the pullout force, to the contact pressure, $P = N/A$, where N is the normal force, between contacting bodies,

$$\mu = \frac{\tau}{P} \tag{3}$$

From experimental observation of an increasing coefficient of friction with increasing velocity and a decreasing coefficient of friction with increasing normal force [11–17], hydrodynamic lubrication can be assumed such that contacting surfaces are fully separated by the viscous film of the thermoplastic matrix. Considering the viscous resistance of the polypropylene film between the composite sample and the metal tooling, the coefficient of friction can be defined as,

$$\mu = \frac{\eta \cdot \dot{\gamma}}{P} \tag{4}$$

where the viscosity, η, of the polypropylene has been defined by the Power Law of Ostwald and de Waele [25],

$$\eta = m\,\dot{\gamma}^{n-1} \tag{5}$$

and where $\boldsymbol{m}$ is the consistency, $\boldsymbol{n}$ is the power-law index, and $\dot{\gamma}$ is the shear-strain rate given by

$$\dot{\gamma} = \frac{U}{h} \tag{6}$$

where $\boldsymbol{U}$ is the velocity and $\boldsymbol{h}$ is the fluid-film thickness. Because power-law parameters for polypropylene are not available in the literature at a temperature of 170°C, the parameters at 180°C (Table 1) are used in the calculation of the resin viscosity. The consistency and power-law index at 180°C are only applicable to shear rates between 100–400 s^{-1}. The velocities generally observed in the thermostamping process [1] and studied here give shear rates within the applicable range assuming a fluid-film thickness of 0.07 mm deduced from optical micrographs [26]. It has been shown that at shear rates between 100–400 s^{-1}, the viscosity of polypropylene is nearly the same as at temperatures of 170 and 180°C (Fig. 7 [16]), justifying the use of the power-law parameters at 180°C.

Substituting Eqs. 5 and 6 into Eq. 4 gives,

$$\mu = \left[\frac{m}{h^n}\right] \cdot \left[\frac{U^n}{P}\right] \tag{7}$$

Equation 7 describes the respective influences of the fluid-film thickness, the velocity and the pressure on the hydrodynamic friction coefficient. The term $\left[\frac{U^n}{P}\right]$ will be referred to as the modified Hersey number in this research. Like the Hersey number, the modified Hersey number takes the inverse effects of velocity and pressure on the effective

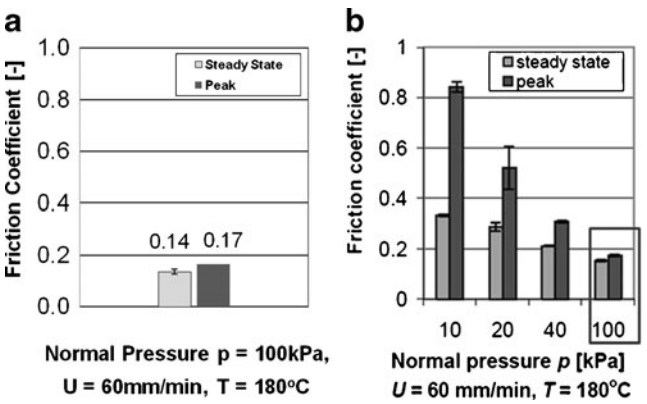

Fig. 6 Friction coefficient measurements from **a** UMass Lowell and from **b** University of Twente as part of an ongoing friction international benchmark exercise [24]

Table 1 Power-law parameters for polypropylene at 180°C [25]

$\dot{\gamma}$ range, s^{-1}	Consistency, m, Ns^n/m^2	Power-law index, n
100–400	6.79×10^3	0.37

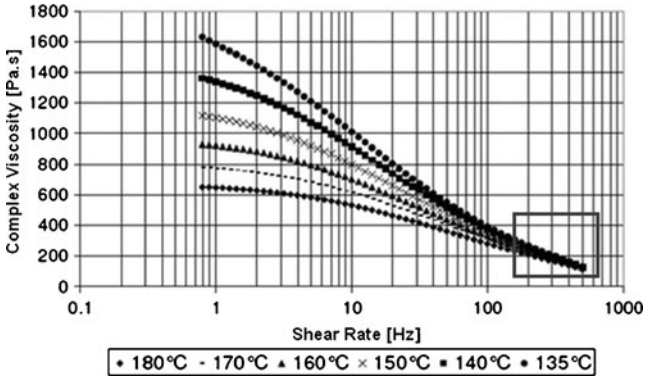

Fig. 7 Flow curves for polypropylene at different temperatures [16]

friction coefficient and groups them into a single parameter. Equal values of modified Hersey numbers should thus theoretically correspond to equal coefficients of friction. Compared to the use of the conventional Hersey number,

$$H = \frac{\eta U}{P} = m\left(\frac{U}{h}\right)^{n-1}\frac{U}{P} \tag{8}$$

the modified Hersey number has the advantage of not needing to assume a specific value for $\boldsymbol{h}$, i.e. the fluid-film thickness. However, the implicit assumptions are that the frictional behavior is hydrodynamic and that the film thickness is uniform over the area of interest for a given modified Hersey number. While there will certainly be a variation in the fluid-film thickness due to height variations in the fabric yarns, an average fluid-film thickness over the fabric area is assumed. Additionally, the calculation of the modified Hersey number requires the input of rheological properties such as the power-law index.

The test matrix shown in Table 2 was developed to observe how different combinations of normal forces and velocities, i.e. different modified Hersey numbers $\left[\frac{U^n}{P}\right]$, affect the friction between the tool and the fabric during the first second that it takes to form the sample to the shape of the die. Two sets of test parameters were chosen for the three modified Hersey numbers investigated.

Table 2 Test conditions studied for Hersey investigation (PW and TW)

Test ID	Modified Hersey number , U^n/P [(m/s)^n/Pa]	Velocity (mm/s)	Pressure (kPa)
A-1	4.38×10^{-7}	8.3	337
A-2	4.38×10^{-7}	16.7	438
B-1	1.11×10^{-6}	16.7	172
B-2	1.11×10^{-6}	10.0	143
C-1	1.98×10^{-6}	25.0	112
C-2	1.98×10^{-6}	16.7	97

Experimental results

All samples were cut to 51 mm×76 mm, and all test conditions were explored in triplicate. The results were plotted with error bars of one standard deviation for the PW and TW fabrics. A symmetric two-layer sample of the PW fabric was used for each test, while a single-layer sample was used for the much-thicker TW fabric. The reason for the difference in the number of layers used in the test is because of the respective thicknesses of the fabrics. The fabric samples must be thick enough such that the thermocouple monitoring the fabric temperature can be sufficiently embedded within the sample. The relatively thin PW fabric would have more voids if only one layer was used and thus the thermocouple may be measuring the tool surface temperature rather than the fabric temperature.

Tool/fabric friction–PW

At the tool/fabric interface, Fig. 8 shows that equal modified Hersey numbers do produce similar dynamic coefficients of friction for the PW fabric, and that an upward trend exists between the modified Hersey number and the dynamic coefficient of friction, similar to the hydrodynamic region of the Stribeck curve. These two observations validate the approach used, in particular the assumptions of hydrodynamic lubrication and constant fluid-film thickness, $\boldsymbol{h}$, for a given modified Hersey number. Equation (7) can be rearranged to solve for a varying fluid-film thickness, $\boldsymbol{h}$, at different combinations of normal load and velocity, from the experimentally obtained coefficients of friction,

$$h = \left[\left[\frac{m}{\mu}\right]\cdot\left[\frac{U^n}{P}\right]\right]^{\frac{1}{n}} \tag{9}$$

The trend observed in the film thickness is consistent with the trend obtained by an analytical model developed

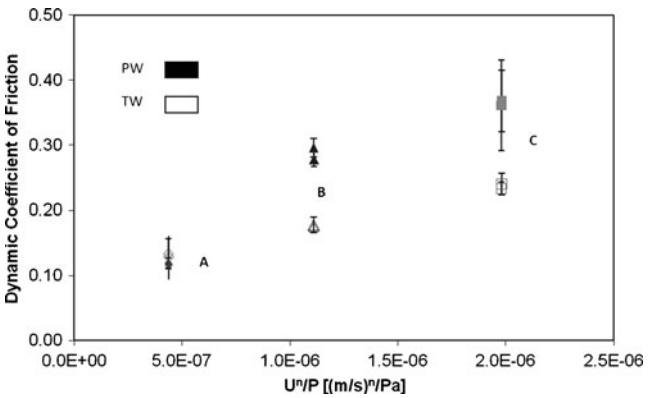

Fig. 8 Dynamic coefficient of friction as a function of modified Hersey number for the PW and TW fabrics (tool/fabric)

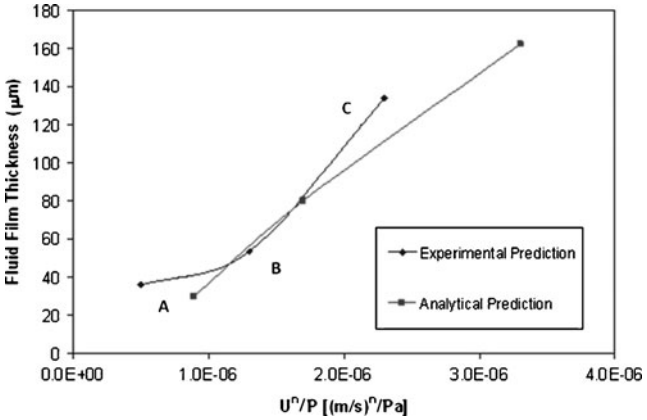

Fig. 9 Comparison of predicted fluid-film thickness between experimental and Ten Thije et al. [17] analytical results

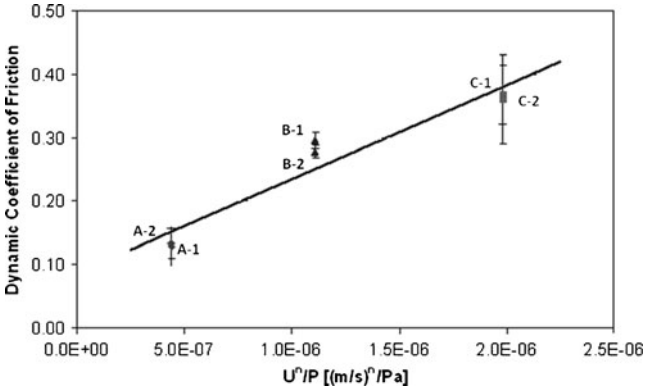

Fig. 11 Example of linear fit through experimental data for the PW fabric (tool/fabric)

by R. Ten Thije et al. [17] that uses Reynolds' equation to determine the fluid-film thickness based on combinations of pressure, velocity, and viscosity. For the same modified Hersey numbers, the order of magnitude of the fluid-film thickness compares well between the analytical model and the predictions based on experimental results (Fig. 9). It should be noted, however, that the analytical model used by R. Ten Thije et al. is for a similar fabric (same yarns) but a different weaving (balanced twill-weave) heated to a temperature of 200°C. Also, the power-law index was estimated based on a plot from Vanclooster et al. [16]. Nevertheless, the similarities in the trends and the orders of magnitude of the fluid-film-thickness between the analytical and experimental results demonstrate the credibility of the approach used in the current research.

Tool/fabric friction—TW

The dynamic coefficient of friction for the TW fabric at the tool/fabric interface as a function of modified Hersey number is also shown in Fig. 8. Although the magnitude of the friction for the TW fabric was generally lower than that for the PW fabric, the increasing trend replicates the hydrodynamic region of the Stribeck curve. The observed lower values demonstrate that the weaving of the fabric and/or the thickness of the yarns can influence the friction coefficient, notably via an effect on the fluid-film thickness. In the hydrodynamic region of the Stribeck curve, $\boldsymbol{h}$ is controlling the friction coefficient for a given modified Hersey number according to Eq. 7. However, it is also believed that the looser weave of the TW fabric allows for more sliding and/or rolling of individual yarns/fibers in the sample as compared to the PW, a phenomenon that is not included in the model and that would decrease the overall resistance to pull, as opposed to the tighter PW samples that were essentially pulled as one whole sheet. Rather than trying to account for this phenomenon in the friction model, it would be more correct to consider this mechanical behavior in a material model of the fabric architecture as a separate work.

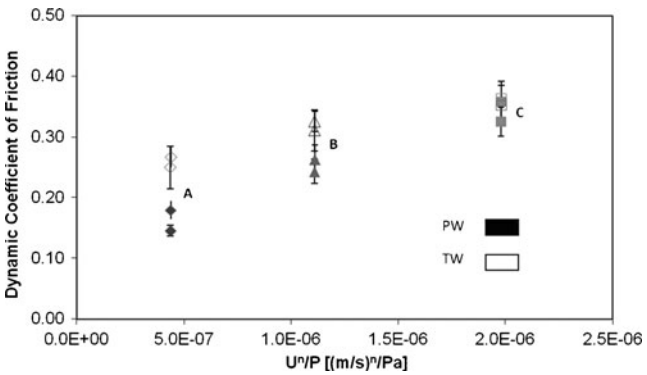

Fig. 10 Dynamic coefficient of friction as a function of modified Hersey number for the PW and TW fabrics (fabric/fabric)

Fabric/fabric friction—PW

When the PW fabric slides against another PW fabric, the friction is observed to increase with increasing modified Hersey number (Fig. 10), which can also be described by the hydrodynamic region of the Stribeck curve. The fabric/fabric friction for the PW fabric was very similar to the tool/fabric coefficient of friction for this fabric as shown previously in Fig. 8—indicating that the thickness of the

Table 3 Phenomenological friction equation coefficients

Fabric type	Contact interface	C_1 [Pa/(m/s)^n]	C_2
PW	Tool/Fabric	0.147	0.087
PW	Fabric/Fabric	0.115	0.116
TW	Tool/Fabric	0.076	0.087
TW	Fabric/Fabric	0.063	0.237

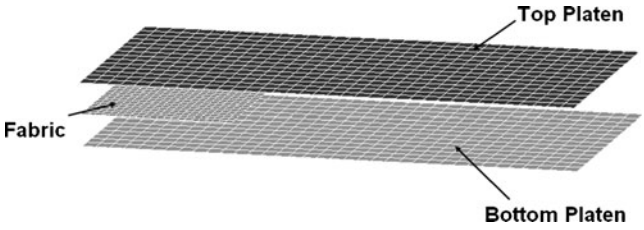

Fig. 12 Exploded view of components of the friction-test finite element model

resin film separating the contacting surfaces is comparable for these two cases per Eq. 7.

Fabric/fabric friction—TW

The frictional behavior of the TW fabric at the fabric/fabric interface is also shown in Fig. 10. For the same modified Hersey number, the fabric/fabric friction was higher than the tool/fabric coefficient of friction for this fabric as shown previously in Fig. 8. The higher friction between adjacent layers of fabric was most likely due to the interlocking of the thick yarns which could:

- lead to a reduced fluid-film thickness,
- limit the yarn/fiber slide and/or roll previously discussed.

The presence of these two phenomena can explain the increase in the overall friction. Relative to the PW fabric at the fabric/fabric interface, the interply friction of the TW fabric was generally higher. It is believed that the thicker TW fabric required more soaking by the heaters for the contacting layers of fabric to be separated by an equivalent amount of resin than was required for the PW fabric. Because more dry fabric was present due to incomplete wetting and the thicker yarns, the overall friction was higher than noted with the PW fabric. Future experiments will investigate preconsolidating the fabrics prior to heating in an attempt to obtain a more complete wetting of the fabric and a possible change in the effective friction coefficient due to the change in wetting.

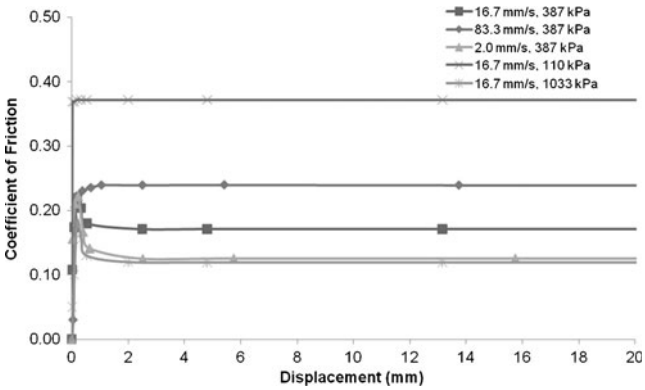

Fig. 14 Typical friction vs. displacement curves from ABAQUS/Explicit friction-test model (PW fabric—tool/fabric)

Finite element models

Implementation of a phenomenological friction law

The commercially available finite element packages ABAQUS/Explicit and LS-DYNA allow for implementation of user-defined frictional behavior via a subroutine (VFRIC in ABAQUS/Explicit and USRFRC in LS-DYNA). The nodal velocities and forces can be used to calculate the modified Hersey number, which corresponds to a particular coefficient of friction. A linear regression of the experimental friction data was used (Fig. 11) to obtain a dynamic friction coefficient dependent on the modified Hersey number. The general form of the equation for μ_d, the dynamic coefficient of friction, can be written as,

$$\mu_d = C_1 \cdot HM + C_2 \tag{10}$$

where HM is the modified Hersey number and is equal to $\left[\frac{U^n}{P}\right]$. The coefficients, C_1 and C_2 are summarized in Table 3 and can be defined directly in the input files. Note that the order of magnitude of the coefficients is adjusted to account for the units used in the finite element codes per the material properties.

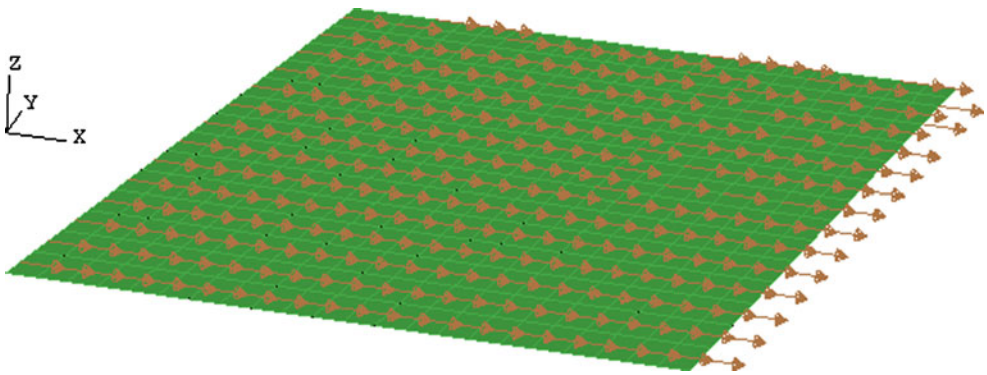

Fig. 13 Prescribed velocity in pull-direction

Validation

A finite element model of the friction experimental setup was run to validate the ability of the proposed friction model to replicate the response of a fabric friction test. This validation would give credibility that a finite element model of a thermostamping simulation would correctly calculate friction based on the normal loads and velocities that can occur during a forming simulation. The finite element model of the friction test consisted of a top platen, bottom platen, and fabric sample mounted in the "rigid" fabric holder (Fig. 12). Surface-to-surface contact was used for this model in both ABAQUS/Explicit and LS-DYNA. Four-noded rigid shell elements were used to model the top and bottom platens, which were assumed to be rigid bodies relative to the fabric. The nodes on the top platen were free to move in the direction of the applied normal load, while the nodes on the bottom platen were completely fixed. The normal load was applied to the top platen.

At the University of Massachusetts Lowell, PW and TW fabric composites have already been experimentally characterized and then modeled with nonlinear constitutive equations being defined via user-defined material subroutines in the explicit versions of ABAQUS and LS-DYNA. The details of the material model are given in Jauffrès et al. [5, 27]. Fabric models are generated using a mesh of 1-D and 2-D elements. The evolution of the shearing of the fabric stiffness is captured by the 2-D elements (shell or membrane elements) and the tensile properties of the fabric yarns are modeled by beam or truss elements in ABAQUS or seatbelt elements in LS-DYNA [5]. The user-defined material model for the PW fabric was used to define the fabric sample in the fabric-friction finite element models.

A pressure equivalent to the pressure used in the friction characterization experiments was applied to the top platen in the first step of the analysis. In the subsequent steps, the pressure was held constant and a velocity was prescribed in the pull-direction on all of the fabric nodes (Fig. 13). To reduce computational time, velocities were scaled up by a factor of 10 or 100 to run an analysis, but accordingly scaled down within the user subroutine by the same factor to calculate the associated effective modified Hersey number.

Table 4 ABAQUS/Explicit friction-test finite element model results (tool/fabric)

Velocity (mm/s)	Pressure (kPa)	Theoretical friction coefficient	VFRIC friction coefficient	% difference
16.7	387	0.171	0.171	0.0
16.7	110	0.383	0.382	0.3
16.7	1033	0.119	0.120	0.8
2.0	387	0.125	0.125	0.0
83.3	387	0.239	0.239	0.0

Table 5 ABAQUS/Explicit friction-test finite element model results (fabric/fabric)

Velocity (mm/s)	Pressure (kPa)	Theoretical friction coefficient	VFRIC friction coefficient	% difference
16.7	387	0.182	0.182	0.0
16.7	110	0.347	0.347	0.0
16.7	1033	0.141	0.141	0.0
2.0	387	0.146	0.146	0.0
83.3	387	0.235	0.231	1.7

ABAQUS/explicit

Using VFRIC and the appropriate coefficients from Table 3, various combinations of pull velocities and normal loads were applied to the friction-test models and the coefficients of friction were plotted as a function of pull displacement (Fig. 14). The range explored corresponds to modified Hersey numbers varying between 2.1×10^{-7} and 2.0×10^{-6}. The theoretical dynamic coefficient of friction is obtained using Eq. 10 and the VFRIC dynamic friction coefficient is computed using Eq. 2 and the finite element model normal and pull-out force outputs. A static-dynamic exponential decay equation (Eq. 11) was used to model the transition from static to dynamic friction,

$$\mu_{eff} = \mu_d + (\mu_s - \mu_d)e^{-\beta\dot{\gamma}} \tag{11}$$

where μ_s is the static friction coefficient and is a function of pressure, β is the decay constant and $\dot{\gamma}$ is the slip rate. The decay constant defines the transition rate from zero velocity to final velocity (static to dynamic friction coefficient). A decay constant of 0.15 was determined to best-fit experimental data points and was thus used in the finite element

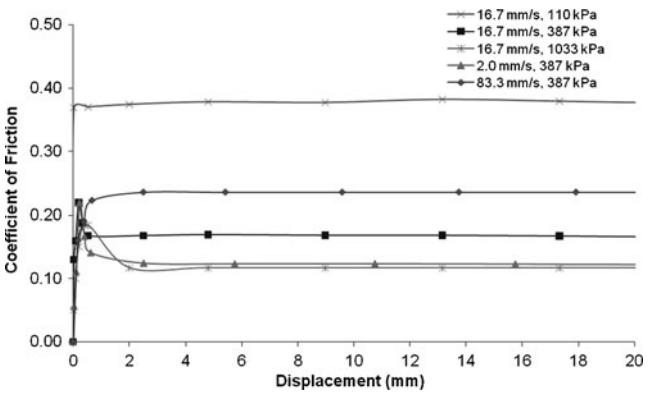

Fig. 15 Typical friction vs. displacement curves from LS-DYNA friction-test model (PW fabric—tool/fabric)

Table 6 LS-DYNA friction-test finite element model results (tool/fabric)

Velocity (mm/s)	Pressure (kPa)	Theoretical friction coefficient	VFRIC friction coefficient	% difference
16.7	387	0.171	0.168	1.8
16.7	110	0.383	0.377	1.6
16.7	1033	0.119	0.117	1.7
2.0	387	0.125	0.123	1.6
83.3	387	0.239	0.235	1.7

models. The dynamic coefficient of friction results (Tables 4 and 5) indicate that VFRIC accurately accounts for changes in velocity and normal force to update the dynamic coefficient of friction as a function of the test conditions. Note that the model is capable of capturing a peak as is associated with the static coefficient and can transition to the dynamic coefficient. However, while the peak as calculated by the model does not necessarily correspond to the experimental data, it will be shown later in this paper that this peak value is found to be unimportant to the simulation of the forming process because the dynamic coefficient of friction is the dominating factor. Further work will be pursued to gain a better understanding of the factors such as pressure, velocity and any others (e.g. acceleration) play in determining the static coefficient by revisiting the test methodology. However, based on the current understanding of the forming process, such a pursuit would be only of academic interest with respect to the application under consideration, i.e. thermostamping.

LS-DYNA

The friction user-defined subroutine, USRFRC, and the coefficients from Table 3 were used to replicate the friction test in LS-DYNA for different combinations of pull velocities and normal loads. The coefficients of friction were plotted as a function of pull displacement (Fig. 15) and the results from the model compared well to theoretical calculations of friction coefficient versus modified Hersey number (Tables 6 and 7).

Table 7 LS-DYNA friction-test finite element model results (fabric/fabric)

Velocity (mm/s)	Pressure (kPa)	Theoretical friction coefficient	VFRIC friction coefficient	% difference
16.7	387	0.182	0.179	1.7
16.7	110	0.347	0.343	1.2
16.7	1033	0.141	0.139	1.4
2.0	387	0.146	0.144	1.4
83.3	387	0.235	0.231	1.7

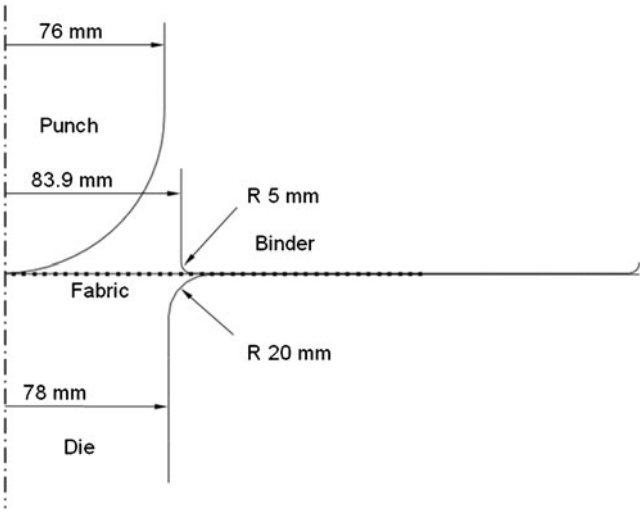

Fig. 16 Deep drawing of a hemisphere: geometry of the tools

Hemisphere forming simulations

After validating the user-supplied subroutines with a finite element model of the friction test, both VFRIC and USRFRC were applied to a single-layer ([0°/90°]) hemisphere model with equal binder pressures and stamping rates. The dimensions of the hemisphere geometry are provided in Fig. 16. The resulting punch forces were compared between ABAQUS/Explicit and LS-DYNA (Fig. 17), and the results agree well with each other. The slight difference between ABAQUS/Explicit and LS-DYNA solutions may be due to different element formulations and contact algorithms within each code and is consistent with other composite forming model comparisons [5].

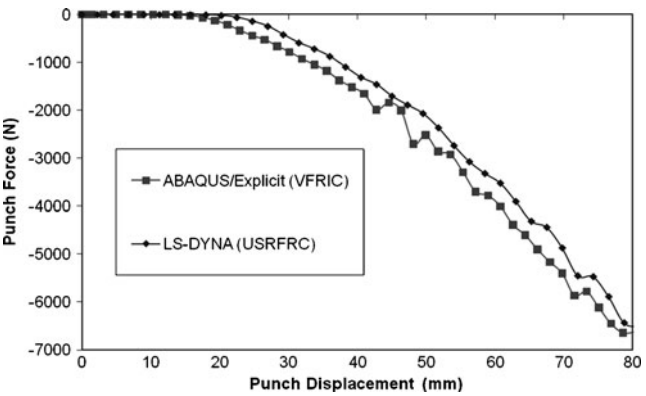

Fig. 17 Comparison of hemisphere model between ABAQUS/Explicit and LS-DYNA for user-defined friction subroutines with a binder pressure of 200 kPa and a stamping rate of 90 mm/s (PW fabric)

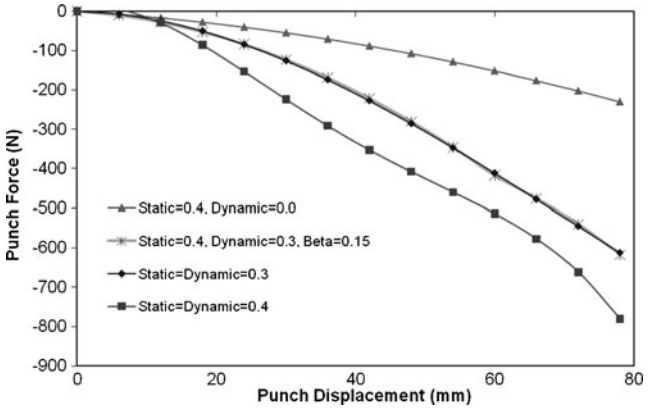

Fig. 18 Sensitivity analysis showing that the static coefficient of friction does not significantly affect the punch forces during a hemispherical forming simulation

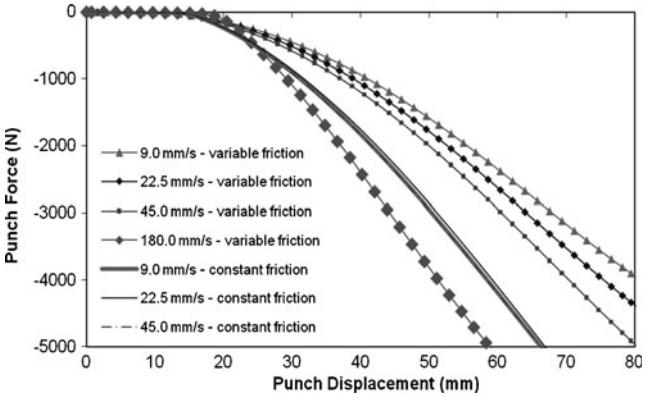

Fig. 19 Punch forces as a result of stamping rate using the PW fabric with variable fabric-friction model and with constant friction coefficient (μ=0.3)

Various forming simulations were run to study the effect of the static coefficient of friction on the punch forces (Fig. 18). As expected, the punch forces are higher when using a constant static and dynamic friction coefficient of 0.4 than when using a constant static and dynamic friction coefficient of 0.3. However, when using a static friction coefficient of 0.4 and a dynamic friction coefficient of 0.3 with Eq. 11, the punch forces are equivalent to those when using a constant friction coefficient of 0.3 throughout the simulation. Alternatively, if the static friction coefficient of friction is 0.4 and the dynamic friction coefficient is 0, the punch forces are very low, due to the lack of a dynamic friction coefficient. This sensitivity analysis shows that for the current friction model using Eq. 11, the dynamic coefficient of friction is the dominant factor in defining the friction behavior of a forming simulation. Thus, the current formulation for the static coefficient of friction being only a function of the normal pressure does not compromise the overall simulation outcome.

The punch force associated with the hemispherical forming process is expected to vary depending on the combination of punch velocity and binder pressure. To explore the effect of stamping rate on the punch force, different stamping rates were applied to the hemisphere model in ABAQUS/Explicit (Table 8) while the binder pressure was maintained at 200 kPa.

Using the stamping rates and the 200-kPa binder pressure as given in Table 8 with a fixed coefficient of friction of 0.3 and then with a rate-dependent coefficient of friction, the resulting punch forces show no dependence on stamping rate for a constant coefficient of friction of 0.3 but show a wide variation with velocity for the rate-dependent coefficient of friction. The results for the two types of friction analyses are shown in Fig. 19. In this figure, it can be seen that if the simulation of this forming process is done using a constant coefficient of friction, the punch force can be either over-predicted or under-predicted relative to the results shown using a variable coefficient of friction, i.e. as a function of the velocity, which based on the friction characterization tests is a more credible way to capture the fabric friction. Alternatively, if the punch velocity is held constant at 45.0 mm/s and the binder pressure is changed from 200 kPa to 20 kPa (Fig. 20), the resulting punch forces are also reduced by a factor of 10 when using a constant friction coefficient. However, the variable friction coefficient leads to slightly higher punch forces relative to a constant friction coefficient at 20 kPa because the friction coefficient has increased with a lower binder pressure (Fig. 20). Figures 19 and 20 show the importance of incorporating a varying friction coefficient

Table 8 Effect of punch velocity on punch force

Simulation No.	Binder Pressure (kPa)	Punch Velocity (mm/s)
1	200	9.0
2	200	22.5
3	200	45.0
4	200	180.0

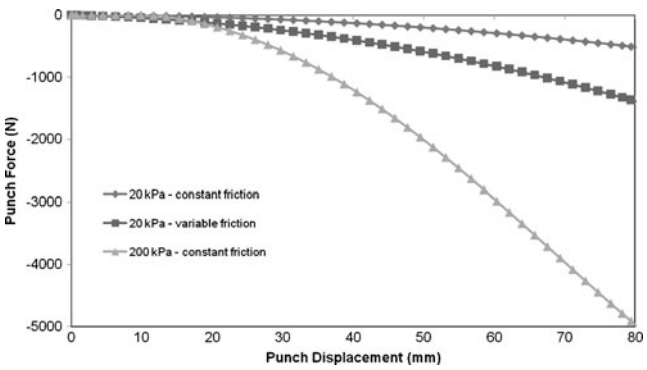

Fig. 20 Punch forces as a result of varying binder pressures using the PW fabric with variable fabric-friction model and with constant friction coefficient (μ=0.3)

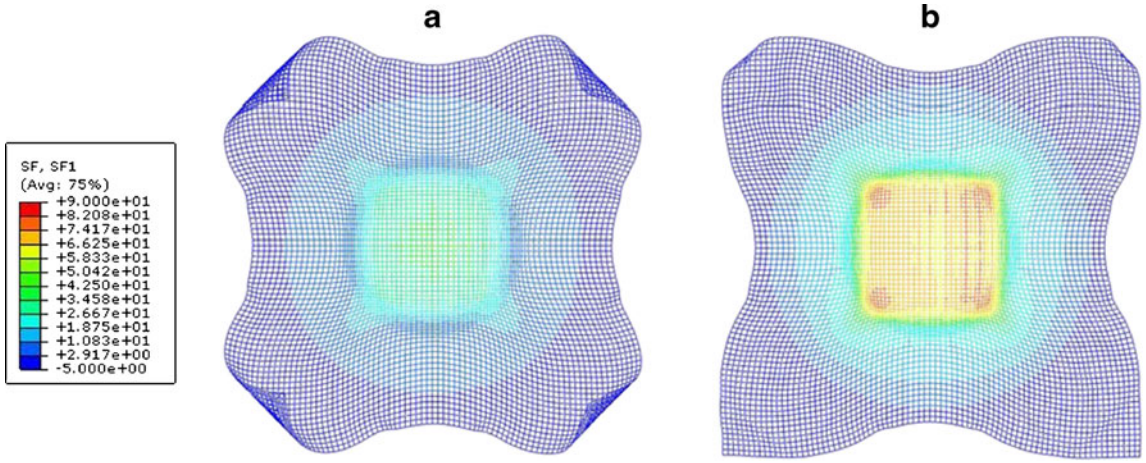

Fig. 21 Tensile stresses in PW fabric yarns **a** with fabric-friction model and **b** with constant friction coefficient (μ=0.3). Both models used stamping rates of 45 mm/s and binder pressure of 200 kPa

that is dependent upon the critical thermostamping process parameters such as the stamping rate and binder pressure.

As stated previously, as the frictional forces increase, the effective in-plane forces increase and consequently the tensile stresses in the yarns increase. If the tensile stresses in the yarns approach the tensile strength of the yarns, then fiber breakage and tearing can occur, thereby compromising the quality of the formed part. Figure 21 shows that assuming a constant coefficient of friction (μ=0.3) shows much higher tensile stresses in the fabric yarns for a punch rate of 45 mm/s than for the same rate using the variable coefficient of friction. Similar to the punch force, the tensile stresses are also under-predicted at elevated velocity (180 mm/s) when using a constant coefficient of friction (μ=0.3) in comparison to the variable friction. For a two-layered part (0/90 and +/−45), the tensile stresses are also over-predicted using a punch rate of 90 mm/s and a constant coefficient of friction (μ=0.3) when compared to the same simulation using a variable coefficient of friction (Fig. 22). Incorrectly predicting the fabric stresses could lead to an improper adjustment of the binder forces and cause unexpected manufacturing defects such as fabric tearing or wrinkles. In addition, a predictive tool incorporating velocity effects on the friction coefficient allows for the optimization of the processing speed, i.e. manufacturing rate. Previous studies have shown that higher tensile stresses do not necessarily affect the manner in which the fabric shears. Instead, fabric shearing is controlled more by the kinematics of the fabric assuming the shape of the mold [12]. Thus, the design of a composite thermostamping process requires a thorough understanding of the fundamental inputs to the effective friction coefficients for an engineer to use the simulation tool effectively. The simple use of a constant coefficient of friction may lead to incorrect conclusions for the processing rates and tool forces.

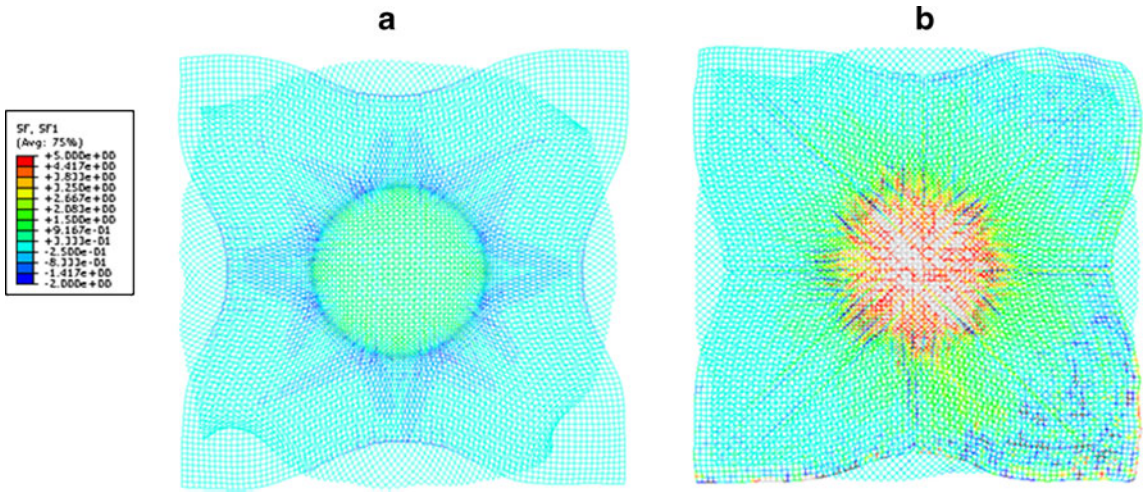

Fig. 22 Tensile stresses in dual-layer (0/90 and ±45) PW fabric yarns (a) with fabric-friction model and (b) with constant friction coefficient (μ=0.3). Both models used stamping rates of 90 mm/s and binder pressure of 200 kPa

Conclusion

A load-control friction test apparatus was used to measure dynamic coefficients of friction of a Twintex® balanced plain-weave (PW) and unbalanced twill-weave (TW) thermoplastic-matrix woven-fabric composite at 170°C. It was shown that equal coefficients of friction were obtained when testing different combinations of normal force and fabric velocity resulting in equal modified Hersey numbers. Thus, the modified Hersey number was used to relate the normal force and velocity to the dynamic coefficient of friction during thermostamping. The modified Hersey number approach developed here allows the back-calculation of the fluid-film thickness, rather than assume a constant value of the fluid-film thickness for all test conditions as it had been done previously.

The experimental data were used to develop a linear regression model between the friction coefficient and the modified Hersey number, and the model was subsequently implemented into finite element codes ABAQUS/Explicit and LS-DYNA via user-defined friction subroutines to capture the hydrodynamic frictional behavior of the fabrics during the thermoforming process. The user-defined friction subroutines were first validated using a finite element model of the experimental friction test. The dynamic coefficients of friction obtained from the finite element simulations correlated well with the theoretical dynamic coefficients of friction for equal Hersey numbers. The user-defined friction subroutines accounted for dynamically changing friction coefficients as a function of variations in the velocity and normal force experienced locally by the fabric.

Hemisphere stamping simulations were performed using constant and variable friction coefficients. The friction at the tool/fabric and fabric/fabric interfaces significantly affected the punch force, as well as the resulting tensile stresses in the fabric yarns. Increasing the stamping rate led to an increase in the friction force at the tool/fabric interface, thus increasing the punch force and the tensile stresses in the yarns. Using a constant coefficient of friction showed that the punch force had no dependence on the stamping rate. Incorrectly predicting the fabric stresses could lead to unexpected manufacturing defects and an incorrect yarn tensile stress as a function of the processing speed, i.e. manufacturing rate.

Acknowledgements This research was partially completed under NSF Award # DMII-0522923. The donation of Twintex® plain-weave fabric by Vetrotex (now owned by Owens Corning) is appreciated.

References

1. Gorczyca J, Sherwood J, Liu L, Chen J (2004) Modeling of friction and shear in Thermostamping process—Part I. J Compos Mater 38:1911–1929
2. Gamache L (2007) The design and implementation of a friction test apparatus based on the thermostamping process of woven-fabric composites. Master's Thesis, Department of Mechanical Engineering, University of Massachusetts Lowell
3. Wilks CE (1999) Characterization of the Tool/Ply interface during forming. Ph.D Thesis, School of Mechanical, Materials, Manufacturing Engineering and Management, University of Nottingham, UK
4. Boisse P, Hamila N, Helenon F, Hagege B, Cao J (2008) Different approaches for woven composite reinforcement forming simulation. Int J Mater Form 1:21–29
5. Jauffrès D, Sherwood JA, Morris CD, Chen J (2010) Discrete mesoscopic modeling for the simulation of woven-fabric reinforcement forming. Int J Mater Form 3:S1205–S1216
6. Willems A (2008) Forming simulation of textile reinforced composite shell structures. Faculteit Ingenieurswetenshapen Arenbergkasteel. Leuven (Belgium): Katholieke Universiteit Leuven, p.281
7. ten Thije RHW*, Akkerman R, Huétink J (2007) Large deformation simulation of anisotropic material using an updated Lagrangian finite element method. Comput Methods Appl Mech Engrg 196:3141–3150
8. Peng XQ, Cao J (2005) A continuum mechanics-based non-orthogonal constitutive model for woven composite fabrics. Comp Part A: Appl Sci Manufact 36:859–874
9. Yu WR, Pourboghrata F, Chungb K, Zampalonia M, Kang TJ (2002) Non-orthogonal constitutive equation for woven fabric reinforced thermoplastic composites. Composites: Part A 33:1095–1105
10. Pickett AK, Creech G, De Luca P (2005) Simplified and advanced simulation methods for prediction of fabric draping. Eur J Comput Mech 14(6–7):677–91
11. Akkerman R, Ubbink MP, de Rooij MB, ten Thije RHW (2007) Tool-ply friction in composite forming. 10th ESAFORM Conference on Material Forming, 1080–1085
12. Fetfatsidis K (2009) Characterization of the tool/fabric and fabric/fabric friction for woven fabrics: Static and Dynamic. Master's Thesis, Department of Mechanical Engineering, University of Massachusetts Lowell
13. Ersoy N, Potter K, Wisnom M, Clegg M (2005) An experimental method to study the frictional processes during composites manufacturing. Compos Part A: Appl Sci Manuf 36:1536–1544
14. Murtagh AM, Lennon JJ, Mallon PJ (1995) Surface friction effects related to pressforming of continuous fibre thermoplastic composites. Compos Manuf 169-175
15. Chow S (2002) Frictional interaction between blank holder and fabric in stamping of woven thermoplastic composites. MS Thesis, Department of Mechanical Engineering, University of Massachusetts Lowell
16. Vanclooster K, Lomov SV, Verpoest I (2008) Investigation of interply shear in composite forming. Proceedings for the 11th ESAFORM Conference on Material Forming. Lyon, France pp 957–960
17. ten Thije RHW, Akkerman R, van der Meer L, Ubbink MP (2008) Tool-ply friction in thermoplastic composite forming. Proceedings for the 11th ESAFORM Conference on Material Forming. Lyon, France, pp 550–553
18. Hutchings IM (1992) Tribology: friction and wear of engineering materials. CRC, Ann Arbor, pp 62–67
19. Gorczyca-Cole J, Sherwood J, Chen J (2007) Development of a friction model for use in the thermostamping of commingled glass-polypropylene woven fabrics. Compos Part A: Appl Sci Manuf 38(2)
20. Akkerman R, ten Thije RHW (2010) Finite element simulations of laminated composites forming processes. Int J Mater Form 38 (2):715–718

21. Fetfatsidis KA, Gamache L, Sherwood JA, Jauffrès D, Chen J (2011) Design of an apparatus for measuring tool/fabric and fabric/fabric friction of woven-fabric composites during the thermostamping process. International Journal of Material Forming, doi 10.1007_s12289-011-1058-3
22. Cao J, Akkerman R, Boisse P, Chen J, Cheng HS, DeGraaf EF, Gorczyca J, Harrison P, Hivet G, Launay J, Lee W, Liu L, Lomov S, Long A, Deluycker E, Morestin F, Padvoiskis J, Peng XQ, Sherwood J, Stoilova T, Tao XM, Verpoest I, Willems A, Wiggers J, Yu TX, Zhu B (2008) Characterization of mechanical behavior of woven fabrics: experimental methods and benchmark results. Composites: Part A 39:1037–1053
23. Lebrun G, Bureau MN, Denault J (2004) Thermoforming-stamping of continuous glass fiber/polypropylene composites: interlaminar and tool-laminate shear properties. J Thermoplast Compos Mater 17:137–165
24. Sachs U, Haanappel S, Rietman B, Akkerman R (2011) Friction testing of thermoplastic composites. Proceedings for the 32nd International SEICO Conference. Paris, France
25. Fried JR (1995) Polymer science and technology. Prentice-Hall, Inc., New Jersey, pp 394–396
26. Clifford MJ, Long AC, deLuca P (2001) Forming of engineering prepregs and reinforced thermoplastics. Presented at the 2001 TMS annual meeting and exhibition, second global symposium on innovations in materials, processing and manufacturing: sheet materials: composite processing, February 11–15
27. Jauffrès D, Sherwood JA, Morris CD, Chen J (2009) Simulation of the thermostamping of woven composites: mesoscopic modelling using explicit FEA codes, Proceedings for the 12th ESAFORM Conference on Material Forming. Twente, Netherlands